http://dx.doi.org/10.5012/bkcs.2012.33.8.2613

Ni(OH)$_2$ and NiO Nanostructures: Synthesis, Characterization and Electrochemical Performance

Lotf Ali Saghatforoush,[*] Mohammad Hasanzadeh,[†,*] Soheila Sanati, and Robabeh Mehdizadeh

Department of Chemistry, Payam Noor University, Tehran, I.R. of Iran. [*]E-mail: saghatforoush@gmail.com
[†]Drug Applied Research Center, Tabriz University of Medical Sciences, Tabriz, Iran
[*]E-mail: mhmmd_hasanzadeh@yahoo.com
Received April 3, 2012, Accepted May 9, 2012

Hydrothermal route have been used in different conditions for preparation of Ni(OH)$_2$ nanostructures. The NiO nanoparticles were obtained by calcining the Ni(OH)$_2$ precursor at 450 °C for 2 h. The effect of sodium dodecyl sulfonate (SDS) as surfactant on the morphology and size of Ni(OH)$_2$ nanoparticles were discussed in detail. X-ray diffraction (XRD), Scanning electron microscopy (SEM), Transmission electron microscopy (TEM) and Fourier transform infrared (FT-IR) spectroscopy were used to characterize the products. The growth mechanism of the as-synthesized nanostructures was also discussed in detail based on the experimental results. Coming up, the NiO nanoparticle modified carbon paste electrode was applied to the determination of captopril in aqueous solution.

Key Words : Ni(OH)$_2$, NiO, Hydrothermal synthesis, Sodium dodecyl sulfonate, Captopril

Introduction

Materials in nanoscale have fascinated the scientific community in the recent years because of their unusual physical and chemical properties compared to those of their bulk counterparts. These materials have potential applications such as catalysts, drug delivery materials, photonic materials, and battery materials.[1-4] The morphology and size of the nanomaterial could greatly influence their optical electronic, magnetic, and catalytic properties.[5-8] Much progress has been made on the size control and morphology control of nanomaterials. Various materials with sizes in the range of several nanometers to micrometers were synthesized[9-12] and a variety of morphologies have also been fabricated such as nanotubules, nanowires, nanorings, ordered hexagonal mesostructures, nanorods, *etc.*[13-17]

Transition-metal hydroxides constitute an important group of mineral materials that have many significant applications. Among these transition-metal hydroxides, nickel hydroxide Ni(OH)$_2$ is an active transition metal hydroxide material used in the positive electrode of alkaline rechargeable batteries for its high power density, high energy, and low toxicity.[18,19] There exist two nickel hydroxide polymorphs: α-phase Ni(OH)$_2$ and β-phase Ni(OH)$_2$. Both have hexagonal layered structures and tend to be thin flakes or platelets in natural/normal formation environments. It has been documented that not only the crystal structure but also the size and morphology of Ni(OH)$_2$ have significant effects on the performance of alkaline rechargeable batteries.[20, 21]

Nickel oxide is a very promising material and has attracted increasing attention due to it's particular catalytic, anomalous electronic and magnetic properties. NiO nanomaterials have been used for a variety of applications including catalysis[22,23] electrochromic windows[24] sensors[25,26] battery cathodes[27] electrochromic films[28,29] and fuel cell electrodes.[30-32] So far, NiO nanostructures with different morphologies such as nanoplates[33] nanowires[34] nanotubes[35] and hollow nanospheres[36] have been obtained.

In this work, we present an effective method to synthesize Ni(OH)$_2$ and NiO nanostructures by decomposition of a nickel complex [Ni(phen)$_2$]Cl$_2$ under hydrothermal conditions with and without the addition of surfactant. The possible formation mechanism of as-prepared NiO was also studied. Also, the electrooxidation of captopril was investigated using NiO nanoparticle-modified carbon paste electrode (NiOM-CPE).

Experimentals

All the chemicals were purchased and used as received without any purification. SEM (Philips XL 30) with gold coating was used to observe the morphologies of Ni(OH)$_2$ and NiO samples. The phase purity of the products was examined by (XRD) using a Rigaku D/max 2500 diffractometer at a voltage of 40 kV and a current of 200 mA with Cu-Kα radiation (k = 1.5406 Å), employing a scanning rate 0.02/s in the 2 h ranging from 5 to 70. FT-IR spectra (4000-400 cm^{-1}) were recorded with a Shimadzu FT-IR Prestige 21 spectrophotometer as KBr disks. Electrochemical measurements were carried out in a conventional three-electrode cell powered by an electrochemical system comprising an AUTOLAB system with PGSTAT12 boards (Eco Chemie, Utrecht, and the Netherlands). The system was run on a PC using GPES 4.9 software. A saturated calomel electrode (SCE) was a reference electrode and auxiliary electrode was a platinum wire. All potentials were measured with respect to the SCE which was positioned as close to the working electrode as possible by means of a luggin capillary.

Table 1. The experimental details of the $Ni(OH)_2$ samples

$Ni(OH)_2$	Chemicals	T/°C	t/h
A	(0.71 g $NiCl_2{\cdot}6H_2O$ + 2 mL distilled water) + (1.18 g 1,10-phenanthroline + 5 mL DW + 1 mL warm ethanol) + 10 mL NaOH (aq, 2 M)	160	24
B	(0.71 g $NiCl_2{\cdot}6H_2O$ + 2 mL distilled water) + (1.18 g 1,10-phenanthroline + 5 mL DW + 1 mL warm ethanol) + 10 mL NaOH (aq, 2 M) + 1.73 g SDS	160	24
C	(0.71 g $NiCl_2{\cdot}6H_2O$ + 2 mL distilled water) + (1.18 g 1,10-phenanthroline + 5 mL DW + 1 mL warm ethanol) + 10 mL NaOH (aq, 2 M)	160	48
D	(0.71 g $NiCl_2{\cdot}6H_2O$ + 2 mL distilled water) + (1.18 g 1,10-phenanthroline + 5 mL DW + 1 mL warm ethanol) + 10 mL NaOH (aq, 2 M) + 1.73 g SDS	160	48

Synthesis of $Ni(OH)_2$ and NiO Samples.

Hydrothermal Synthesis: Nickel hydroxide nanoparticles were obtained by means of hydrothermal synthesis with and without the addition of surfactant. In a typical synthesis, 3 mmol (0.71 g) of $NiCl_2{\cdot}6H_2O$ was dissolved in 2 mL of distilled water. In the other beaker, 6 mmol (1.18 g) of 1,10-phenanthroline was dissolved in 5 mL of distilled water and 2 mL of warm ethanol. Then this solution was added in to the solution of nickel chloride to form a pink solution. 10 mL of NaOH aqueous solution (2 M) was added in to the pink solution and the color of the solution was turned to the light yellow. Finally at reactions which were used from SDS as surfactant, 6 mmol (1.73 g) of SDS was added in to the final solution. The final solution was transferred to a 25 mL Teflon-lined autoclave and heated. Syntheses were carried at 160 °C for 24 and 48 h. After cooling to room temperature, the resulting products was centrifuged, washed with distilled water and ethanol for several times, and dried under vacuum at room temperature to get the sample of β-$Ni(OH)_2$. To obtain NiO the as-prepared sample of β-$Ni(OH)_2$ was calcined in air for 2 h. The detailed parameters of the experiments are shown in Table 1.

Preparation of NiO Modified Carbon Paste Electrode: Bare carbon paste electrode (B-SDS CPE) was prepared by hand-mixing carbon powder and mineral oil (Nujol) (60/40 w/w %) ratio. The paste was carefully mixed and homogenized in an agate mortar for 25 min. The resulting paste was kept at room temperature in a desiccator. The paste was packed firmly into a cavity (3.6 mm diameter, geometric surface area of 0.1017 cm^2 and 0.5 mm depth) at the end of a Teflon tube. Electrical contact was established *via* a copper wire connected to the paste in the inner hole of the tube. The electrode surface was gently smoothed by rubbing on a piece of weighing paper just prior to use. This procedure was also used to regenerate the surface of the carbon paste electrodes. The NiO nanoparticle-modified carbon paste electrodes (NiOM-CPEs) were prepared by mixing carbon powder together with NiO nanoparticles at different ratios in an agate mortar until a uniform paste was obtained. The percentage (w/w) of nickel oxide informed throughout the text corresponds to the final percentage relative to the total paste composition. Then mineral oil was added (40 w/w %) and mixed thoroughly. The paste obtained was packed into a 3 mm diameter cavity at the end of a Teflon tube, and the electrical contact was provided with a copper wire.

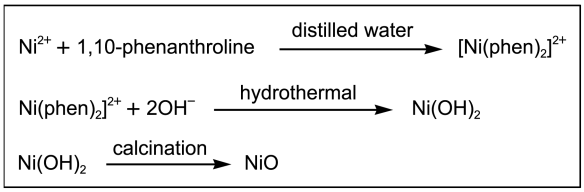

Scheme 1. Illustration of the formation mechanism of NiO.

Results and Discussion

Formation Mechanism. In the beginning Ni^{2+} in solution reacts first with 1,10-phenanthroline to form a relatively stable complex, $[Ni(phen)_2]Cl_2$.[37] Then the solution of NaOH (2 M) was added to provide OH^- ions for the formation of $Ni(OH)_2$ by a hydrothermal treatment. At the end this precursor was calcinated to form NiO nanoparticles. Based on the experimental results, the possible formation mechanism of the NiO nanomaterials was illustrated in Scheme 1.

Hydrothermal Synthesis of $Ni(OH)_2$ with and without Surfactant. The FT-IR spectra for A-D samples shown in Figure 1 reveals chemical information and major functional groups in the $Ni(OH)_2$. The sharp peak at 3640 cm^{-1} is assigned to the stretching vibrational mode (νOH) of non-hydrogen bonded hydroxyl groups in the nickel hydroxide, while the broad band at 3447 cm^{-1} to the stretching mode of hydrogen bonded hydroxyl groups in the same layered structure. The peak at 519 cm^{-1} is attributed to the in plane deformation vibration of water (νOH) and the shoulder absorption at 490 cm^{-1} to the stretching vibration of Ni-OH (νNi-OH).[38] Powder XRD characterizations confirm that $Ni(OH)_2$ nanocrystallites of hexagonal phase have been obtained under our experimental conditions with high purity and high crystallinity. Figure 2 shows the XRD patterns of the samples prepared under different experimental conditions. All the peaks in Figure 2 can be indexed as hexagonal phase β-$Ni(OH)_2$ according to JCPDS card No 14-0117. No characteristic peaks of impurities or other precursor compounds were observed. As shown in Figure 2 when the reaction time increases, the diffraction peaks show stronger intensity which indicates that higher reaction time somewhat improves the crystallinity of the products. The size and morphology of precursors were investigated by SEM and

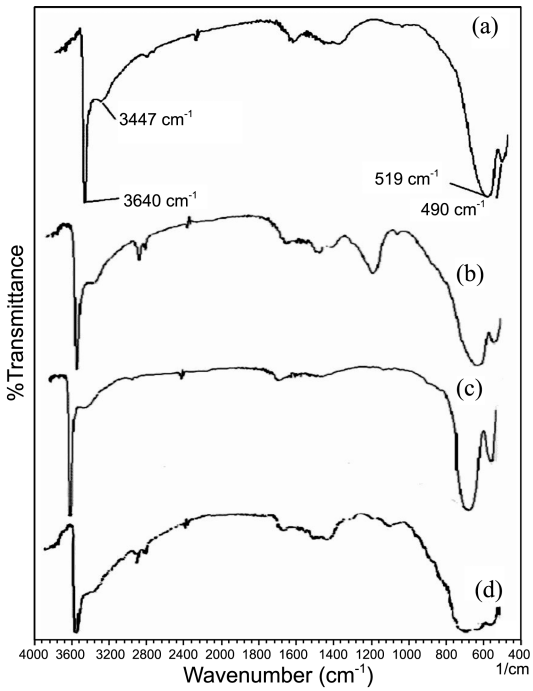

Figure 1. FT-IR spectrums of β-Ni(OH)$_2$ precursors prepared in the different hydrothermal conditions: (a) 160 °C, 24 h, without SDS, (b) 160 °C, 24 h, with SDS, (c) 160 °C, 48 h, without SDS, (d) 160 °C, 48 h, with SDS.

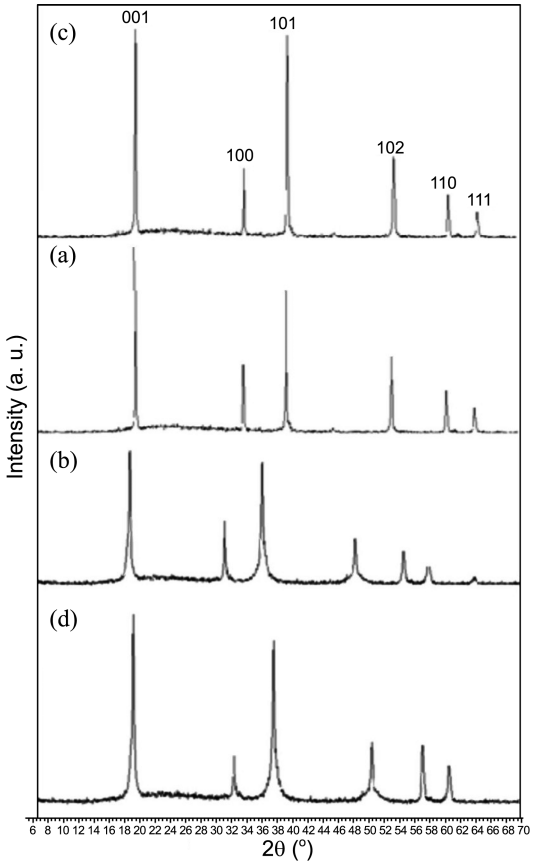

Figure 2. XRD patterns of β-Ni(OH)$_2$ precursors prepared in the different hydrothermal conditions: (a) 160 °C, 24 h, without SDS, (b) 160 °C, 24 h, with SDS, (c) 160 °C, 48 h, without SDS (d) 160 °C, 48 h, with SDS.

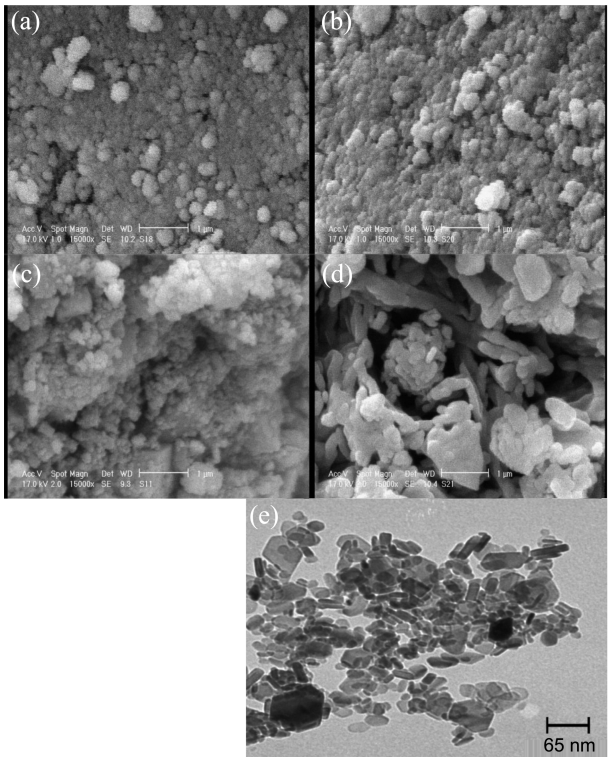

Figure 3. The SEM images of β-Ni(OH)$_2$ precursors prepared in the different hydrothermal conditions: (a) 160 °C, 24 h, without SDS, (b) 160 °C, 24 h, with SDS, (c) 160 °C, 48 h, without SDS (d) 160 °C, 48 h, with SDS and (e) TEM images of β-Ni(OH)$_2$ (e) 160 °C, 48 h, with SDS.

TEM. Figure 3 shows SEM and TEM images of the samples of A-D. The effect of synthesis conditions on morphology development was experimentally investigated and it was found that the presence of SDS together with high reaction time conditions was somewhat effective for the morphology of nanostructures. As shown in Figure 3 under late synthesis conditions the morphology of β-Ni(OH)$_2$ nanostructures was changed from nanoparticle to plate-like morphology. The morphology of the resulting rod-like nanostructures of β-Ni(OH)$_2$ was examined by TEM. From the TEM image (Fig. 3(e)), β-Ni(OH)$_2$ nanostructures with average size of 65 nm were observed.

The average particle size of the samples A and C is about 65 nm and 43 nm and the average particle size of the samples B and D is about 68 nm and 75 nm, respectively. In the presence of SDS as surfactant, the plate-like nanostructures form dense agglomerate and particle size was increased. As shown in Figure 3 the influence of different conditions on morphology and size of β-Ni(OH)$_2$ nanostructures is not very intense.

After heat treatment at 450 °C for 2 h, the -Ni(OH)$_2$ for B and C samples have been transformed into nickel oxide which was indicated as BO and CO, respectively. Figure 4 shows the FT-IR spectra of NiO nanoparticles of the samples of BO and CO. The FT-IR spectra of the NiO show absorption peaks at 3440 cm^{-1} are assigned to the stretching vibration of hydroxyl group. Peaks around 430 cm^{-1} is

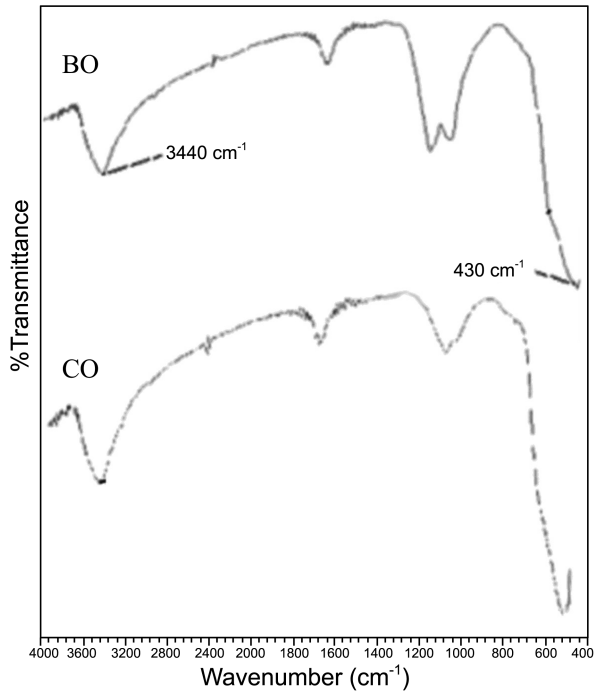

Figure 4. FT-IR spectrums of NiO: (BO) 160 °C, 24 h, with SDS, (CO) 160 °C, 48 h, without SDS.

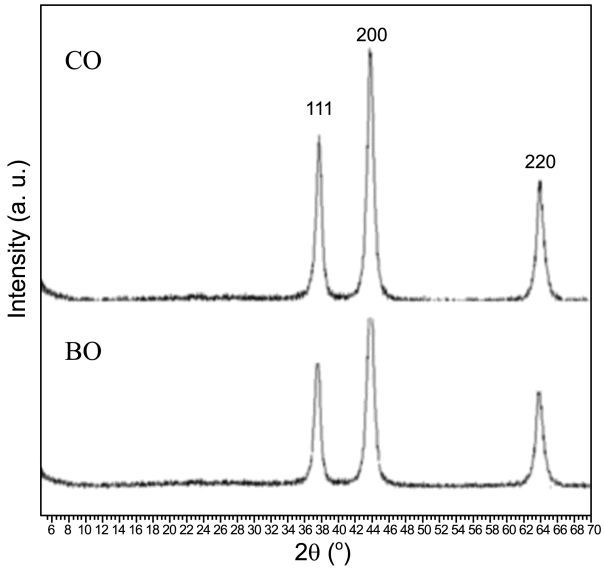

Figure 5. XRD patterns of NiO: (BO) 160 °C, 24 h, with SDS, (CO) 160 °C, 48 h, without SDS.

ascribed to the Ni-O stretching mode.[39] Also, the spectrum of NiO shows the disappearance of any bands assigned to the organic moiety, indicating the complete decomposition of the precursor at 450 °C. Powder XRD characterizations confirm that NiO nanocrystallites of cubic phase have been obtained under our experimental conditions with high purity and high crystallinity. Figure 5 shows the XRD patterns of the NiO samples. All of the reflection peaks in the XRD patterns match well with the standard pattern of cubic NiO (JCPDS card No: 47-1049).[40] No peaks due to β-Ni$(OH)_2$ are observed, suggesting that β-Ni $(OH)_2$ is completely converted to NiO after being heated for 2 h.

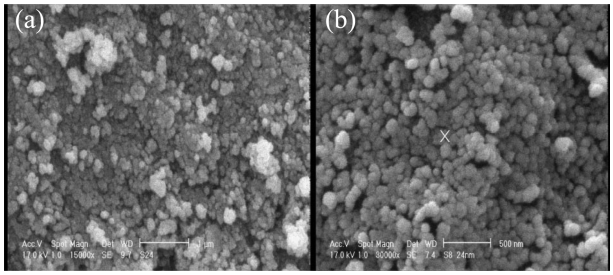

Figure 6. The SEM images of NiO: (BO) 160 °C, 24 h, with SDS (a), (CO) 160 °C, 48 h, without SDS (b).

Figure 6 show the SEM images of the NiO samples BO and CO, which was obtained from samples B and C. As shown in Figure 6 the influence of different conditions on morphology and size of NiO nanostructures is not very intense.

Electrochemical Performance of NiO.

Cyclic Voltammograms of Captopril: The electrochemical oxidation of captopril was performed using the NiOM-CPE. Electrochemical behavior of captopril was investigated on NiOM-CPE by cyclic voltammetry in phosphate buffer solution (pH=5.5). There were no observable peaks for captopril at bare carbon paste signifying it did not accumulate at the electrode surface and the electrochemical reaction was very slow. At NiO nanoparticles modified electrode, however, two anodic peaks occurred. One was at about 0.02 V and another at about 0.6 V (*versus* SCE). As in a blank solution no peaks appeared, it could be inferred that captopril effectively accumulated at modified electrode surface and its electrochemical oxidation was promoted (Fig. 7). At the same time, the background current became larger due to the increased electrode surface. As it can be seen, the peak at about 0.78 V was much higher and sensitive, so it was favorable for captopril determination. With the potential cyclic repeating, the anodic peak current decreased rapidly. Therefore, the voltammograms corresponding to the first cycle were generally recorded.

Influence of Scan Rate: With scan rate increasing, the peak current grows and peak potential shifts positively. There is an excellent linear relationship between peak current and

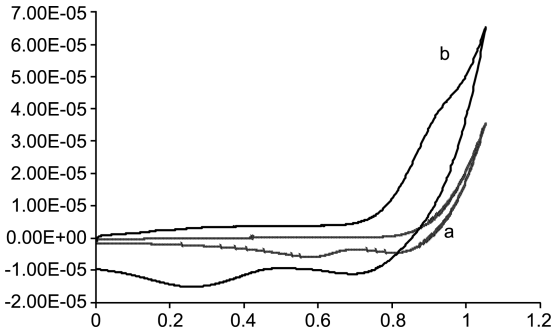

Figure 7. Cyclic voltammograms of bare carbon paste (a) and NiOM-CPE (b) in a 0.55 μM captopril solution. Scan rate: 75 mV s^{-1}.

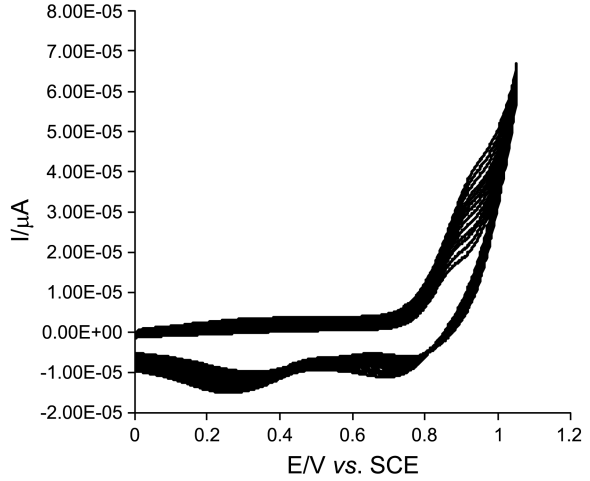

Figure 8. Cyclic voltammograms of NiOM-CPE (b) in a 10 μM captopril solution on different Scan rates: 10-300 mV s^{-1}.

scan rate from 35-170 mV s^{-1} (Fig. 8). The regression equation is i_p = 1.9012 v − 14.335 (r = 0.9768), indicating the electrode process is controlled by adsorption. In addition, the peak potential and the log v shows a linear relationship, following the equation: $E_{p,a}$ = 0.21+0.32 ln$v$, R^2 = 0.981), which suggests the oxidation process is irreversible. The invisible or smaller cathodic peak at CV also can confirm this point.

Influence of Accumulation Time and Accumulation Potential: The effects of accumulation potential on the anodic peak currents of captopril solution were examined over the range −0.6 to 0.4 V. As it is shown in the Figure 9(a), the peak current of captopril in potential range of −0.6 to −0.34 V were increased and after that almost leveled off at increasingly positive potentials. Thus the accumulation potential of −0.34 V was selected as the optimum accumulation potential for further experiments. Figure 9(b) shows plots of the differential pulse anodic peak currents *versus*

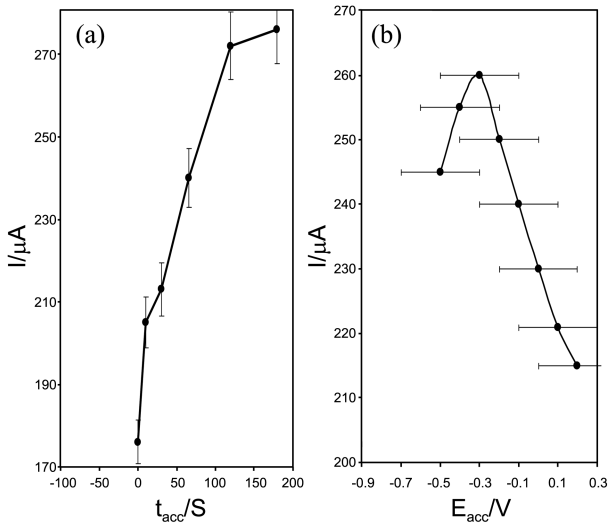

Figure 9. (a) Effect of accumulation time on the peak current of captopril in the phosphate buffer (pH=5.5). (b) Effect of accumulation potential on the peak current of captopril in the phosphate buffer (pH=5.5).

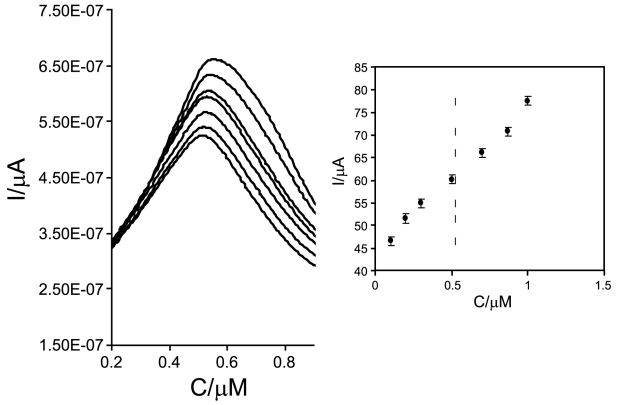

Figure 10. Differential pulse voltammograms obtained with a NiOM-CPE of 0.1, 0.2, 0.3, 0.5, 0.7, 0.9, 1 μM captopril. Inset is calibration curve of captopril.

accumulation time for captopril solution. At first peak current for captopril increase with accumulation time up to 110 s, however after 110 s of accumulation time, the peak current search a plateau. As a consequence, the accumulation time of 110 s was chosen as an optimum time for further experiments.

Calibration Curve: Determination of captopril solutions of different concentrations was carried out by differential pulse voltametry (DPV) (Fig. 10). There was a good linear relationship observed between the anodic peak current and the concentration from 0.1 to 1 μM. The regression equation was i_p = 44.398 + 31.885$C_{captopril}$, R^2 = 0.9912).

Conclusion

In summary, we have successfully synthesized NiO nanostructures with α-Ni(OH)$_2$ as a precursor under different hydrothermal conditions. SDS as surfactant somewhat was effective on the morphology of β-Ni(OH)$_2$ samples. We expect that this method of precursor thermal decomposition can be extended to synthesize of other kinds of metal oxides by using corresponding precursors. NiOM-CPE was applied to the determination of captopril in aqueous solution. The results indicated that NiOM-CPE can increase anodic peak currents by adsorption of captopril on the electrode surface. In addition, it's observed that NiOM-CPE facilitate the determination of captopril.

Acknowledgments. We are grateful to Payam Noor University for financial support of this work and Drug Applied Research Center, Tabriz University of Medical Sciences.

References

1. Li, Z. Q.; Ding, Y.; Xiong, Y. J.; Yang, Q.; Xie, Y. *Chem. Commun.* **2005**, *7*, 918.
2. Dinsmore, A. D.; Hsu, M. F.; Nikolaides, M. G.; Marquez, M.; Bausch, A. R.; Weitz, D. A. *Science* **2002**, *298*, 1006.
3. Zhong, Z. Y.; Gates, Y. D.; Xia, B. Y. *Adv. Mater* **2000**, *12*, 206.
4. Lee, K. T.; Jung, Y. S.; Oh, S. M. *J. Am. Chem. Soc.* **2003**, *125*,

5652.
5. Klimov, V.; Annu, I. *Rev. Phys. Chem.* **2007**, *58*, 635.
6. Li, L.; Hu, J.; Yang, W.; Alivisatos, A. P. *Nano Lett.* **2001**, *1*, 349.
7. Kovtyuklhov, N. I.; Mallouk, T. E. *Chem. Eur.* **2002**, *J8*, 4354.
8. Zhu, J. X.; Gui, Z.; Ding, Y. Y.; Wang, Z. Z.; Hu, Y.; Zou, M. Q. *J. Phys. Chem.* **2007**, *C111*, 5622.
9. Han, D. Y.; Yang, H. Y.; Shen, C. B.; Zhou, X.; Wang, F. H. *Powder Technol.* **2004**, *147*, 113.
10. Lenggoro, I. W.; Yoshifumi, I.; Noritaka, I.; Kikuo, O. *Mater. Res. Bull*. **2003**, *38*, 1819.
11. Zhao, B.; Bao, J. H.; Chen, H. L. *Chin. J. Inorg. Chem*. **2006**, *56*, 17.
12. Haruta, M. *Catal. Today* **1997**, *36*, 153.
13. Liu, H. J.; Peng, T. Y.; Zhao, D. E.; Dai, K.; Peng, Z. H. *Mater. Chem. Phys.* **2004**, *87*, 81.
14. Yang, O.; Sha, J.; Ma, X. Y.; Yang, D. R. *Mater. Lett.* **1967**, *59*, 2005.
15. Liang, J. H.; Li, Y. D. *Chem. Lett.* **2003**, *32*, 1126.
16. Sumit, B.; Ashwin, S.; Aruna, D.; Rao, P. M. *Langmuir* **2003**, *19*, 5522.
17. Wang, W.; Liu, Y.; Xu, C.; Zheng, C.; Wang, G. *Chem. Phys. Lett.* **2002**, *362*, 119.
18. Liang, Z. H.; Zhu, Y. J.; Hu, X. L. *J. Phys. Chem. B* **2004**, *108*, 3488.
19. Wang, D. B.; Song, C. X.; Hu, Z. S.; Fu, X. J. *J. Phys. Chem. B* **2005**, *109*, 1125.
20. CaiF, S.; Zhang, G. Y.; Chen, J.; Gou, X. L.; Liu, H. K.; Dou, S. X. *Angew Chem. Int. Ed*. **2004**, *43*, 4212.
21. Yang, L. X.; Zhu, Y. J.; Tong, H.; Liang, Z. H.; Wang, W. W. *Cryst Growth Des.* **2007**, *7*, 2716.
22. Wang, D. S.; Xu, R.; Wang, X.; Li, Y. D. *Nanotech.* **2006**, *17*, 979.
23. Tost, R. M.; Gonzalez, J. S.; Torres, P. M.; Castellon, E. R.; Lopez, A. J. *J. Mater. Chem.* **2002**, *12*, 3331.
24. Boschloo, G.; Hagfeldt, A. *J. Phys. Chem. B* **2001**, *105*, 3039.
25. Mattei, G.; Mazzoldi, P.; Post, M. L.; Buso, D.; Guglielmi, M.; Martucci, A. *Adv. Mater.* **2007**, *19*, 561.
26. Dirksen, J. A.; Duval, K.; Ring, T. A. *Sens Actuators B* **2001**, *80*, 106.
27. Yoshio, M.; Todorov, Y.; Yamato, K.; Noguchi, H.; Itoh, J.; Okada, M.; Mouri, T. J. *J. Power Sources* **1998**, *74*, 46.
28. Karlsson, J.; Roos, A. *Sol Energy* **2000**, *68*, 493.
29. Fantini, M. C. A.; Ferreira, F. F.; Gorenstein, A. *Solid State Ionics* **2002**, *152-153*, 867.
30. Wang, X.; Li, L.; Zhang, Y. G.; Wang, S. T.; Zhang, Z. D.; Fei, L. F.; Qian, Y. T. *Cryst Growth Des.* **2006**, *6*, 2163.
31. Mamak, M.; Coombs, N.; Ozin, G. A. *Chem. Mater.* **2001**, *13*, 3564.
32. Poizot, P.; Laruelle, S.; Grugeon, S.; Dupont, L.; Tarascon, J. M. *Nature* **2000**, *407*, 496.
33. Ni, X. M.; Zhao, Q. B.; Zhou, F.; Zheng, H. G.; Cheng, J.; Li, B. B. *J. Cryst. Growth* **2006**, *289-299*, 33.
34. Wu, Z. Y.; Liu, C. M.; Guo, L.; Hu, R.; Abbas, M. I.; Hu, T. D.; Xu, H. B. *J. Phys. Chem. B* **2005**, *109*, 2512.
35. Malandrino, G.; Perdicaro, L. M. S.; Fragala, I. L.; NigroR, L.; Losurdo, M.; Bruno, G. *J. Phys. Chem. C* **2007**, *111*, 3211.
36. Sun, X. M.; Liu, J. F.; Li, Y. D. *Chem. Eur. J.* **2006**, *12*, 2039.
37. Masaaki, T.; Toshihiro, M.; Kousuke, K.; Ying, G. W. *Inorg. Chim. Acta* **2005**, *358*, 1823.
38. Oliva, P.; Leonardi, J.; Laurent, J. F.; Delmas, C.; Braconnier, J. J.; Figlarz, M.; Fievet, F.; de Guibert, A. *J. Power Sources* **1982**, *8*, 229.
39. Salavati-Niasari, M.; Mohandes, F.; Davar, F.; Mazaheri, M.; Monemzadeh, M.; Yavarinia, N. *Inorg. Chim. Acta* **2009**, *362*, 3691.
40. Yang, D.; Wang, R.; He, M.; Zhang, J.; Liu, Z. *J. Phys. Chem. B* **2005**, *109*, 7654.